

Electronic Supplementary Information

Switching on Palladium Catalyst Electrochemical Removal from a Palladium Acetate-Acetonitrile System via Trace Water Addition

Haytham E. M. Hussein,^a Andrew D. Ray,^b and Julie V. Macpherson^{a*}

^aDepartment of Chemistry, University of Warwick, Coventry, CV4 7AL, United Kingdom

^bPharmaceutical Technology and Development, AstraZeneca, Macclesfield, SK10 2NA, United Kingdom

* E-mail: j.macpherson@warwick.ac.uk

Table of contents

Section	Description	Page
ESI 1	XRD and NMR analysis of Pd-acetate in CDCl ₃ and MeCN	S2
ESI 2	Understanding the solvation structure of Pd-acetate, Pd ²⁺ and the acetate group using IR and UV-Vis spectroscopy	S4
ESI 3	Electrochemical and microscopy investigation of Pd-acetate in MeCN and water	S5
ESI 4	NMR study of the effect of water addition on Pd-acetate dissolved in MeCN	S8
ESI 5	IR study of MeCN-water system in the presence of Pd-acetate and TBABF ₄	S9
ESI 6	Electrochemistry of Pd-acetate in different MeCN-water mixtures and electrodeposition of Pd	S13
ESI 7	Chemical synthesis of 4-acetylbiphenyl (Suzuki reaction)	S14
ESI 8	Electrochemical recovery of Pd from the synthesis solution	S15
ESI 9	Experimental, methodology and materials	S16
ESI 10	Notes and references	S17

ESI 1: XRD and NMR analysis of Pd-acetate in CDCl₃ and MeCN

Powder XRD was used to determine the solid structure of the powdered form of Pd-acetate¹ as shown in Fig. S1a and Table S1. Trimeric Pd-acetate results in a strong XRD peak $2\theta = 12$, Fig. S1a.

Pd-acetate dissolved in deuterated chloroform (CDCl₃) results in a dominant peak at 2.001 ppm in the ¹H NMR spectrum, as shown in Fig. S1b. This peak corresponds to H in the acetate group (acetate = COOCH₃ = Ac).² The presence of additional smaller peaks (labelled *) of different intensities, indicates hydrolysis of the Pd-acetate compound in CDCl₃ due to trace water impurities, and can be assigned to Pd₃(μ-OH)(OAc)₅.^{2,3} In acetonitrile (MeCN) a single ¹H NMR peak (due to the acetate group) is observed, Fig. S2, shifted downfield to a higher ppm value (2.169 ppm) due to the stronger solvation properties of MeCN compared to CDCl₃ as a result of the presence of a more electronegative element (N).³ The peaks at 1.97 ppm are due to q-MeCN. Both NMR spectra indicate that Pd-acetate retains its cyclic trinuclear structure in solution as signatures associated with free acetate groups do not exist.

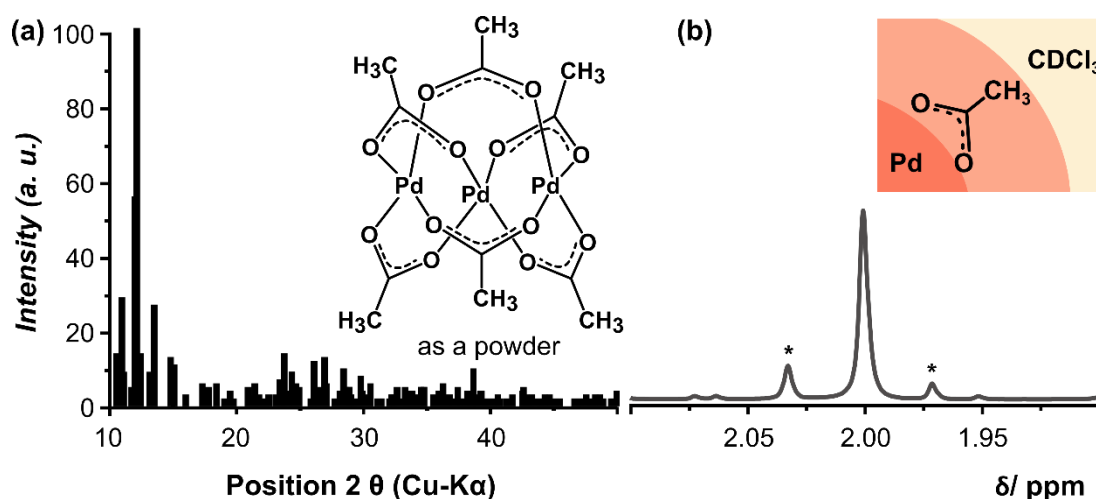


Fig. S1: (a) XRD pattern recorded for trimeric Pd-acetate (Pd₃(OAc)₆). (b) ¹H NMR spectrum taken at 500 MHz in a solution of CDCl₃ containing 1 mM Pd-acetate.

Table S1. List of angles, and the corresponding intensity and lattice planes of trimeric Pd-acetate ($\text{Pd}_3(\text{OAc})_6$).

2θ [°]	i [%]	H	k	L
10.555	13	0	0	2
10.97	28	0	1	2
12.002	55	0	4	0
12.143	100	0	2	2
12.46	13	1	1	-2
13.508	26	1	2	-2
14.802	12	1	3	0
15.079	10	1	3	-2
23.747	13	2	3	-1
23.747	13	1	6	-3
26.096	11	0	5	4
26.933	12	1	8	0
27.066	5	1	4	-5
28.417	9	1	7	2

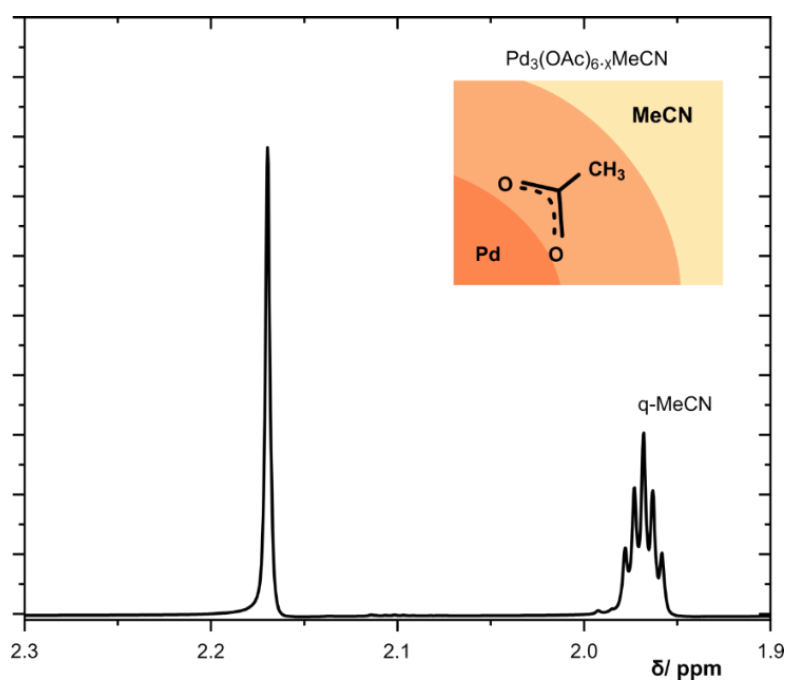


Fig. S2. ^1H NMR spectrum taken at 500 MHz in MeCN containing 1 mM Pd-acetate.

ESI 2: Understanding the solvation structure of Pd-acetate, Pd²⁺ and the acetate group using IR

IR spectroscopy can be used to probe solvent-solvent interactions and ion-solvent interactions.^{4, 5} Coordination of MeCN and acetate anions to the Pd centre can cause measurable shifts in the IR modes *i.e.* shift of the peaks associated with CH₃ bending and stretching to a higher or lower wavenumber based on its coordination. Fig. S3 shows the IR spectra of MeCN (black line) and Pd acetate in MeCN (red line). On (a) and (b) the various vibrational bonds have been identified. In Figure S3c, P1 and P2 represent the C≡N stretch in MeCN and in MeCN containing dissolved Pd-acetate, respectively.

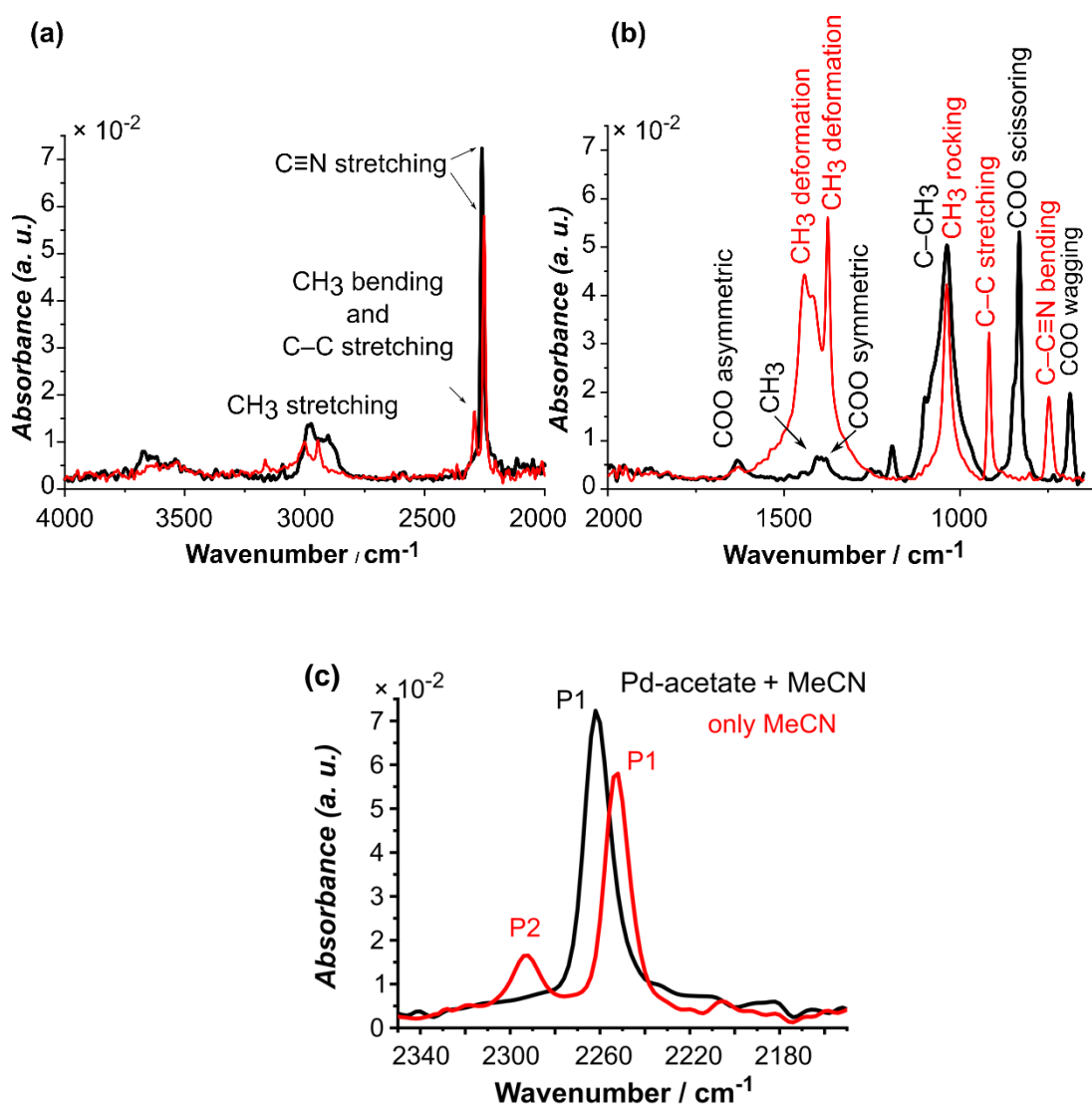


Fig. S3. IR absorption spectra of MeCN (red line) and 1 mM Pd-acetate in MeCN (black line) in the regions (a) 4000 cm⁻¹ to 2000 cm⁻¹; (b) 2000 cm⁻¹ to 700 cm⁻¹; and (c) 2345 cm⁻¹ to 2160 cm⁻¹.

ESI 3: Electrochemical and microscopy investigation of Pd-acetate in MeCN and water

Fig. S4 shows repeat cycling (four cycles) of the electrode, after the first cycle shown in Fig. 1 (main text) for 1 mM Pd-acetate in (a) water (pH 1.8) only and (b) MeCN only, plus supporting electrolyte.

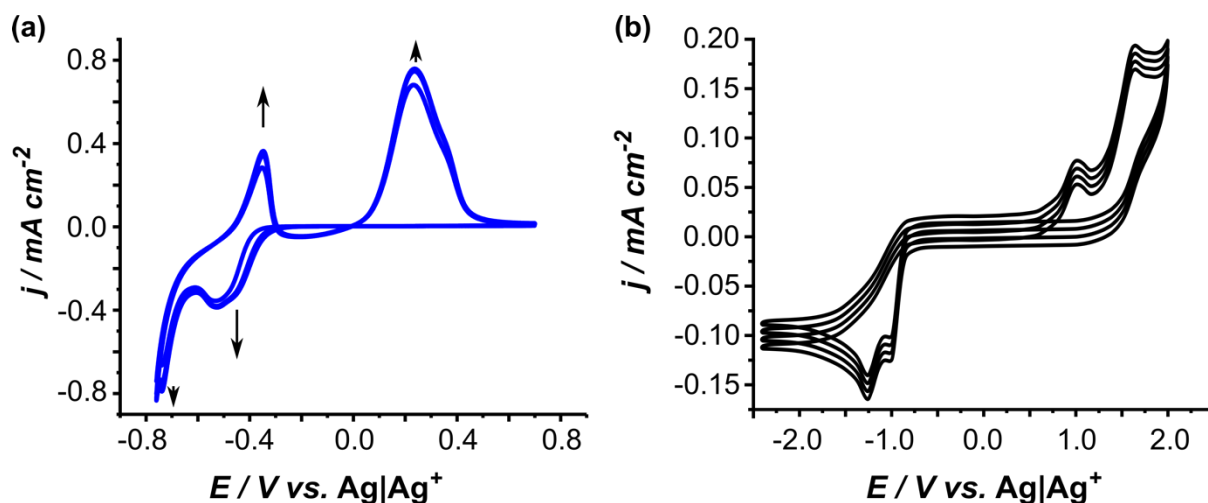


Fig. S4. CVs in a solution containing (a) 1 mM Pd-acetate + 0.1 M HCl + 0.05 M KCl (pH = 1.8) at $v = 0.1 \text{ V s}^{-1}$, and (b) 1 mM Pd-acetate + 0.1 M TBABF₄ in MeCN only at $v = 0.1 \text{ V s}^{-1}$ (in absence of oxygen). Note the first cycle for each is shown in Fig. 1a and b (main text), respectively. The four cycles in (b) are offset for clarity as they sit on top of one another.

Fig. S5 and S6 show (a) chronoamperometric data and (b,c) BDD electrode surface analysis, post electrochemical reduction of Pd-acetate in water and MeCN solutions respectively.

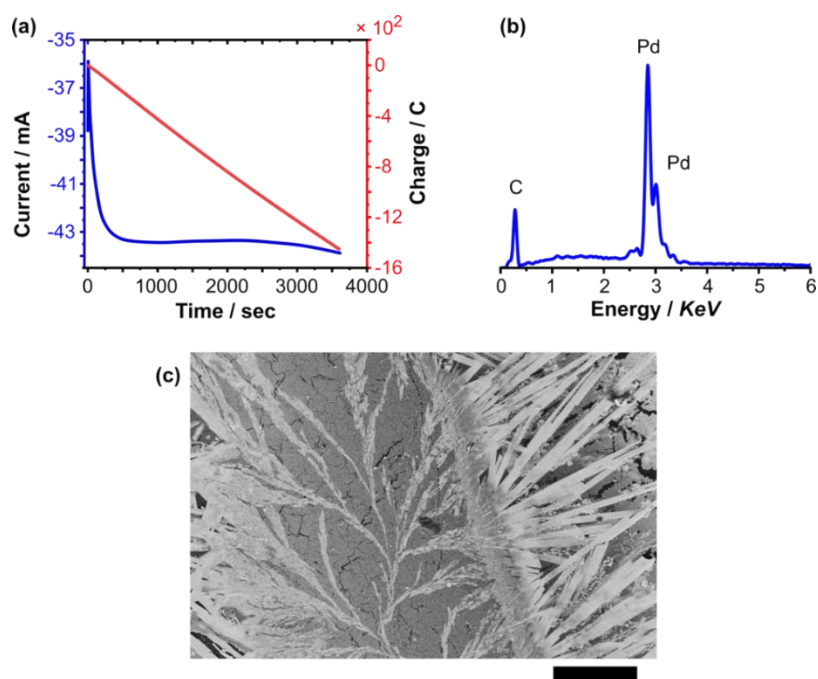


Fig. S5. (a) i - t transient for Pd electrodeposition from a solution containing 1×10^{-3} M Pd-acetate + 0.1 M HCl + 0.05 M KCl at a BDD electrode at $\eta = -1$ V for $t_{dep} = 3600$ s. (b) EDX fingerprint and (c) FE-SEM image of the Pd deposit. Scale bar = 100 μ m.

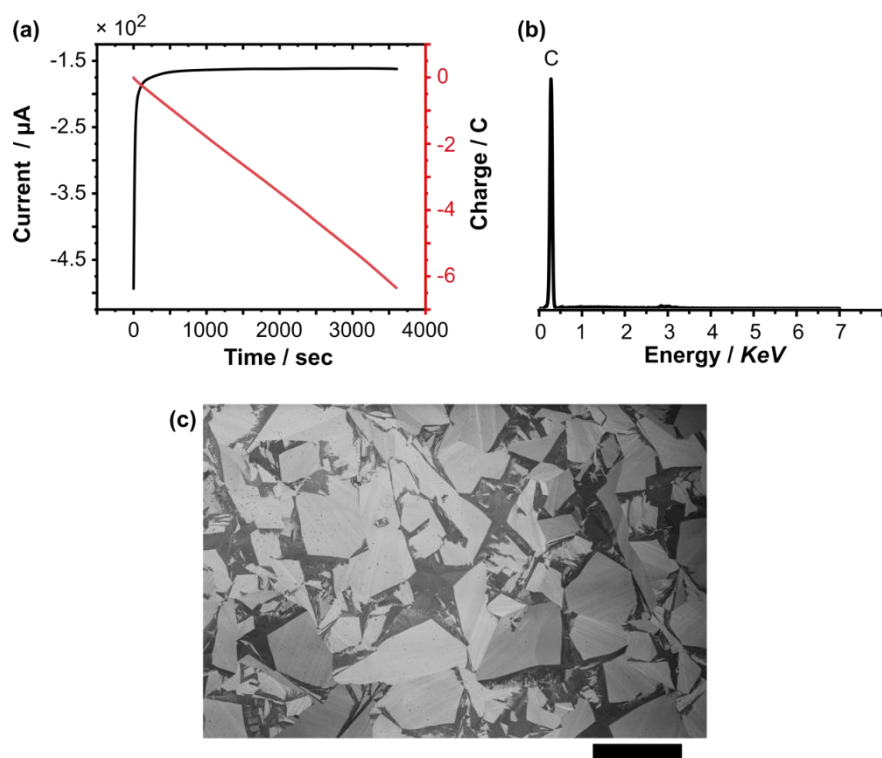


Fig. S6. (a) i - t transient for Pd electrodeposition from solution containing 1×10^{-3} M Pd-acetate + 0.1 M TBABF₄ in MeCN only obtained at a BDD electrode at $\eta = -1$ V for $t_{dep} = 1$ hour. (b) EDX fingerprint and (c) FE-SEM micrograph of the surface. Scale bar = 100 μm .

ESI 4: NMR study of the effect of water addition on Pd-acetate dissolved in MeCN

^1H NMR spectrum of (a) 1 mM $\text{Pd}(\text{CH}_3\text{CN})_4(\text{BF}_4)_2$, (b) 1 mM Pd-acetate in MeCN solution only. Pd co-ordinated to MeCN in $\text{Pd}(\text{MeCN})_4(\text{BF}_4)_2$ shows two peaks at 1.99 ppm and 2.255 ppm. The 2.255 ppm peak shifts downfield in the presence of acetate complexing Pd ligands.

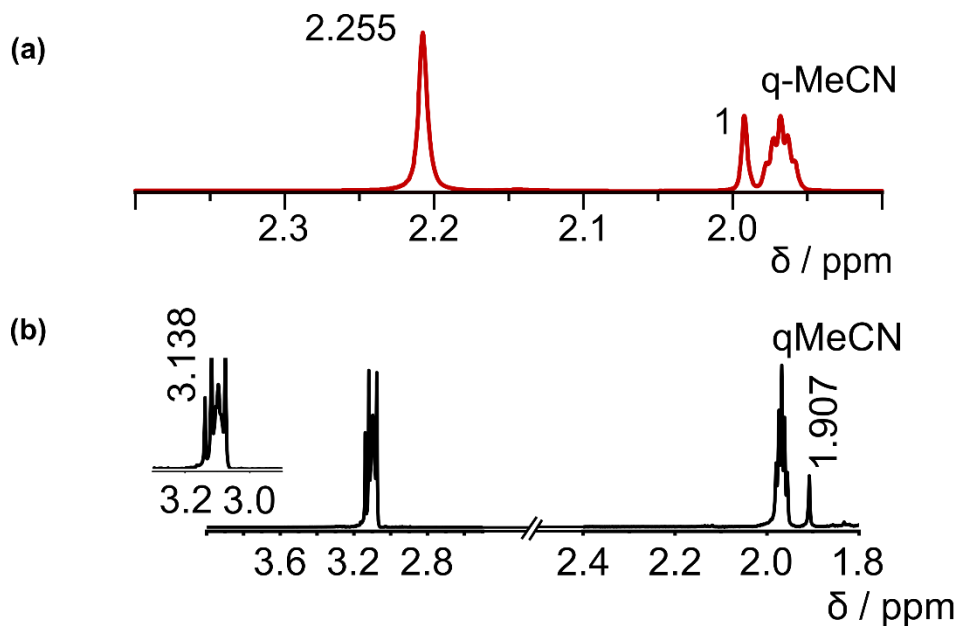


Fig S7. ^1H NMR spectrum of (a) 1 mM $\text{Pd}(\text{CH}_3\text{CN})_4(\text{BF}_4)_2$, (b) 1 mM Pd-acetate in MeCN solution only, (c) 1 mM Pd-acetate after dissolving in solution made of $\chi_{\text{MeCN}} = 0.257$ and $\chi_{\text{water}} = 0.743$ (50%:50% MeCN: water, v/v).

ESI 5: IR study of MeCN-water system in the presence of Pd-acetate and TBABF₄

The premise of the study is to monitor IR wavenumber shifts as function of χ_{water} in MeCN-water mixed solvent and Pd-acetate / TBABF₄.⁶ The water contains 20% D₂O. Fig. S8 exhibits sharp IR bands between 1150 cm⁻¹ and 1000 cm⁻¹ in MeCN only, attributed to the C-CH₃ bond in acetate bound Pd. These sharp peaks start to broaden and coalesce as a function of increasing χ_{water} due to ligand exchange and breaking of the Pd-acetate structure by hydrolysis of the acetate group.

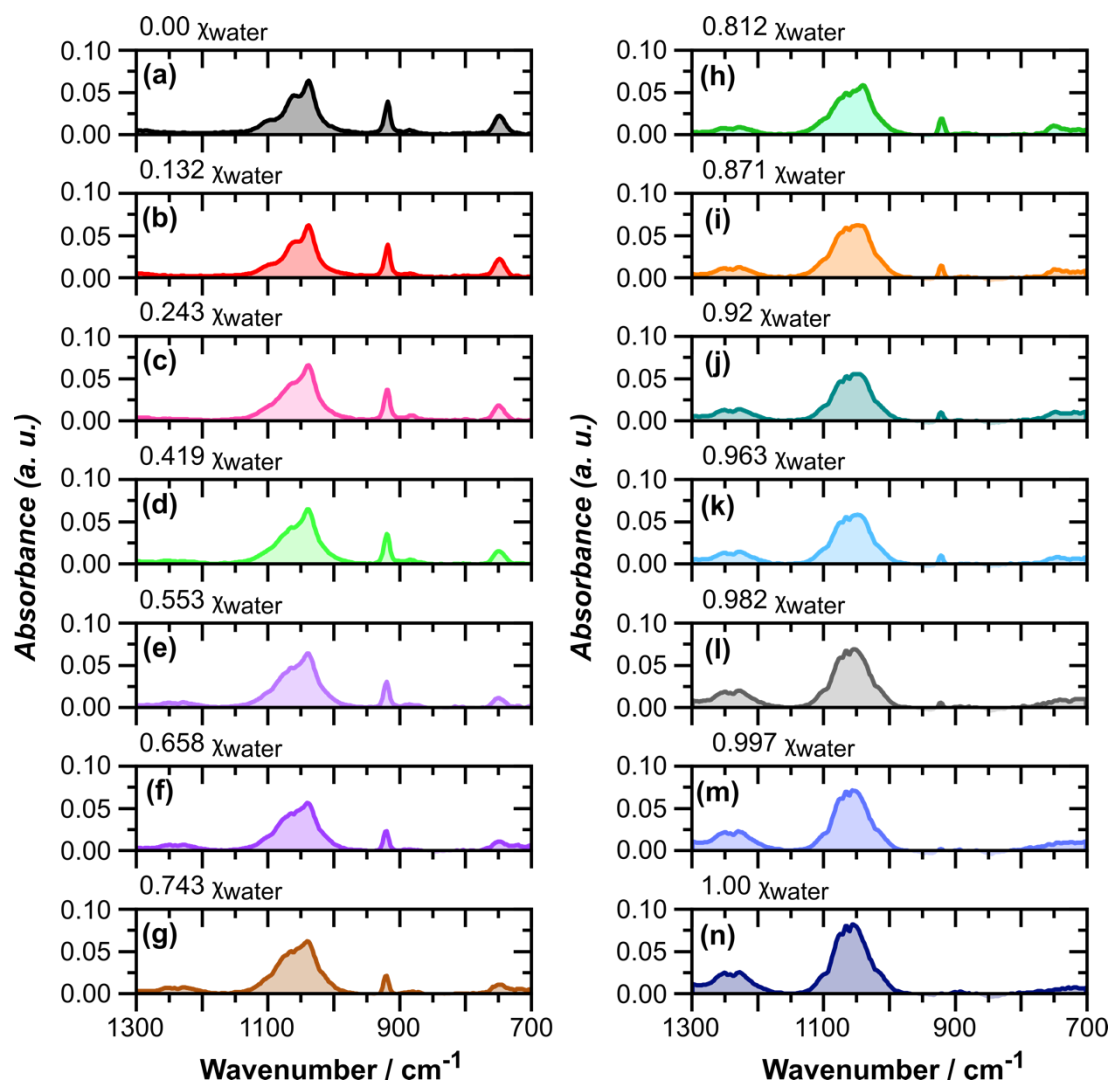


Fig. S8. IR absorption spectra from 1300 cm⁻¹ to 700 cm⁻¹ of MeCN:water mixtures containing 1 mM Pd-acetate + 0.1 M TBABF₄ as a function of increasing water mole fraction ($\chi_{\text{H}_2\text{O}}$) from $\chi_{\text{H}_2\text{O}} = 0.00$ to 1.00. The water contains 20 % D₂O.

In Fig. S9, over the wavenumber range 2320 cm^{-1} to 2220 cm^{-1} , the wavenumber shift of the $\text{C}\equiv\text{N}$ stretching mode (at 2251.9 cm^{-1}) is monitored as a function of increasing χ_{water} from 0.00 to 1.00. This reflects the extent of H-bond formation between MeCN and water molecules. Similarly, we monitor the IR band of CH_3 bending at 2292.7 cm^{-1} , as a function of χ_{water} which represents the presence of free (unbound) MeCN molecules.

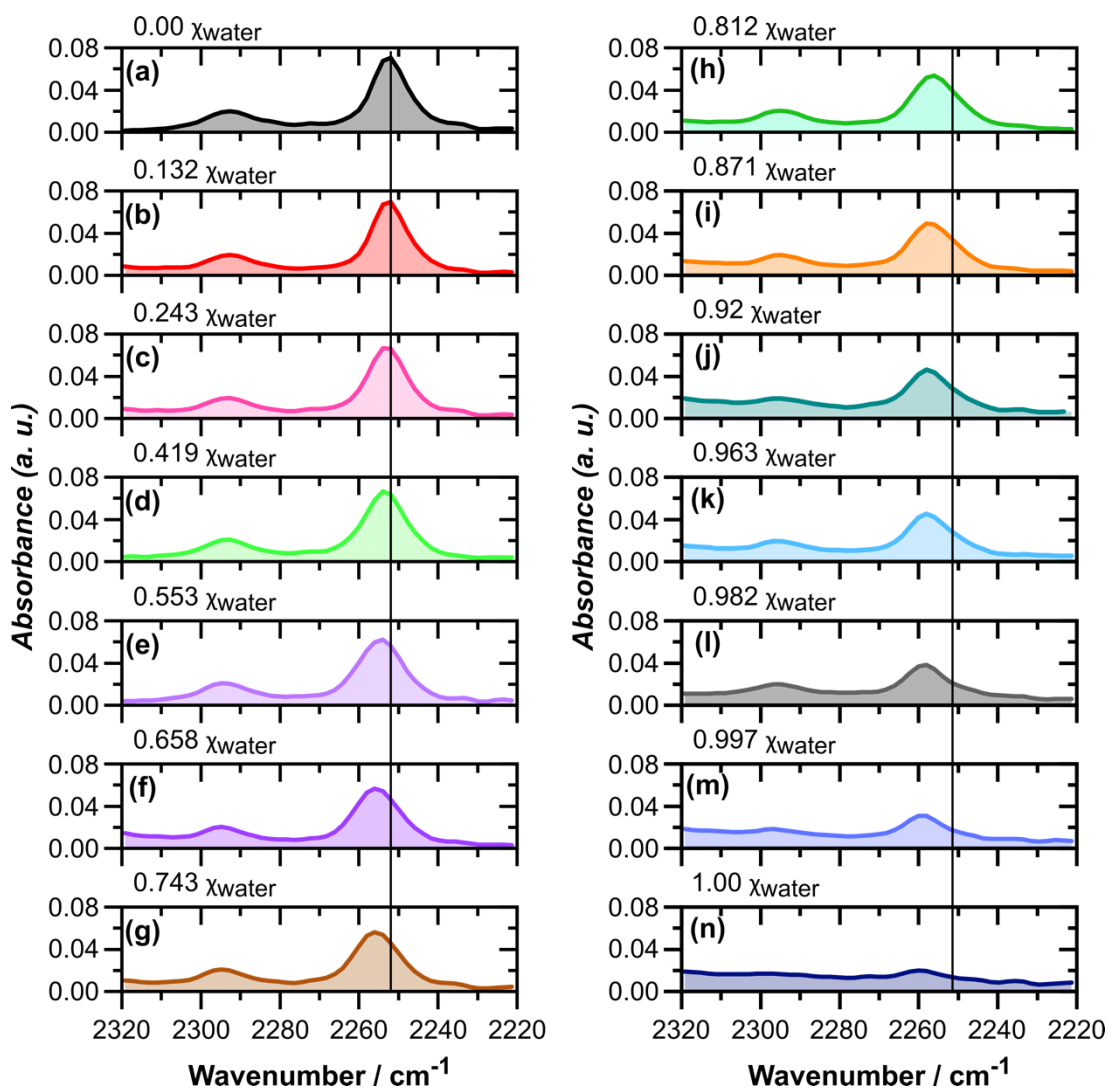


Fig. S9. IR absorption spectra from 2320 cm^{-1} to 2220 cm^{-1} of MeCN:water mixtures containing 1 mM Pd-acetate + 0.1 M TBABF₄ as a function of increasing water mole fraction ($\chi_{\text{H}_2\text{O}}$) from $\chi_{\text{H}_2\text{O}} = 0.00$ to 1.00. The water contains 20 % D₂O.

The wavenumbers of the C≡N and the O-D stretching modes were plotted as a function of χ_{water} in Figs. S10b and 10c. By increasing χ_{water} , Figs. S9 and S10a, the IR band of the C≡N stretching mode shifts to a higher wavenumber, attributed to the formation of hydrogen-bonded MeCN-water molecules and the IR band associated with MeCN molecules not associated with water (2292.7 cm^{-1}) starts to diminish. Akin to previous studies,⁶⁻⁸ the O-D stretch is not observed for MeCN-water mixtures containing $\chi_{\text{water}} < 0.419$. For increasing χ_{water} the O-D band associated with the O-D stretch appears and shifts to lower values with increasing χ_{water} . This behaviour is due to formation of a water network and progressive weakening of the O-D bond, as the network increases in size with increasing χ_{water} .⁶

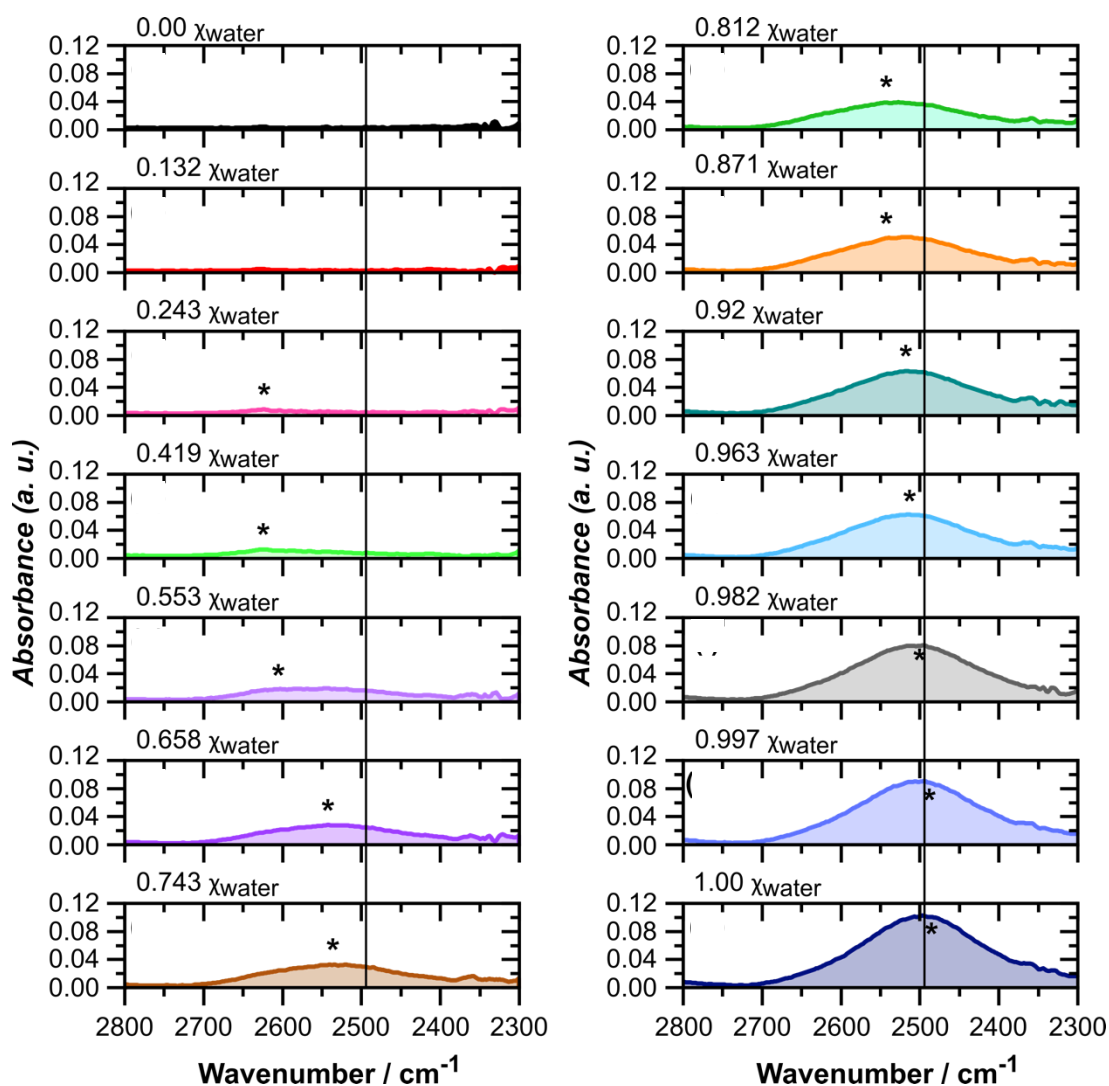


Fig. S10a. Infra-red (IR) absorption spectra from 2800 cm^{-1} to 2300 cm^{-1} of MeCN:water mixtures containing $1 \times 10^{-3} \text{ M}$ Pd-acetate + 0.1 M TBABF₄ as a function of increasing water mole fraction (H_2O) from $\chi_{\text{H}_2\text{O}} = 0.00$ to 1.00 . The water contains 20 % D₂O

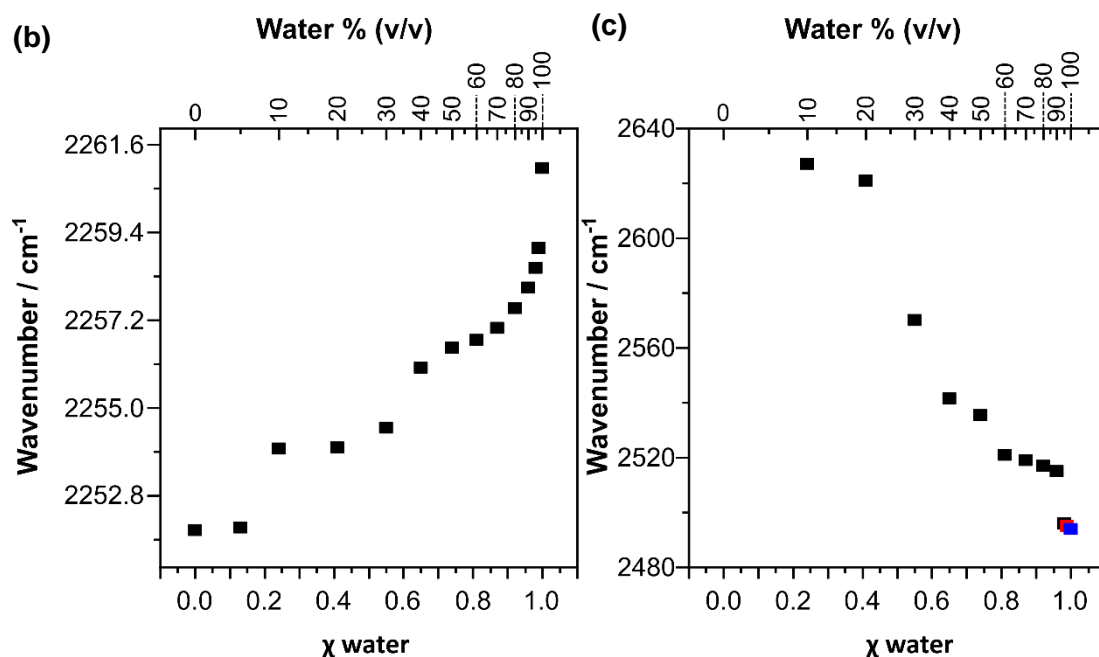
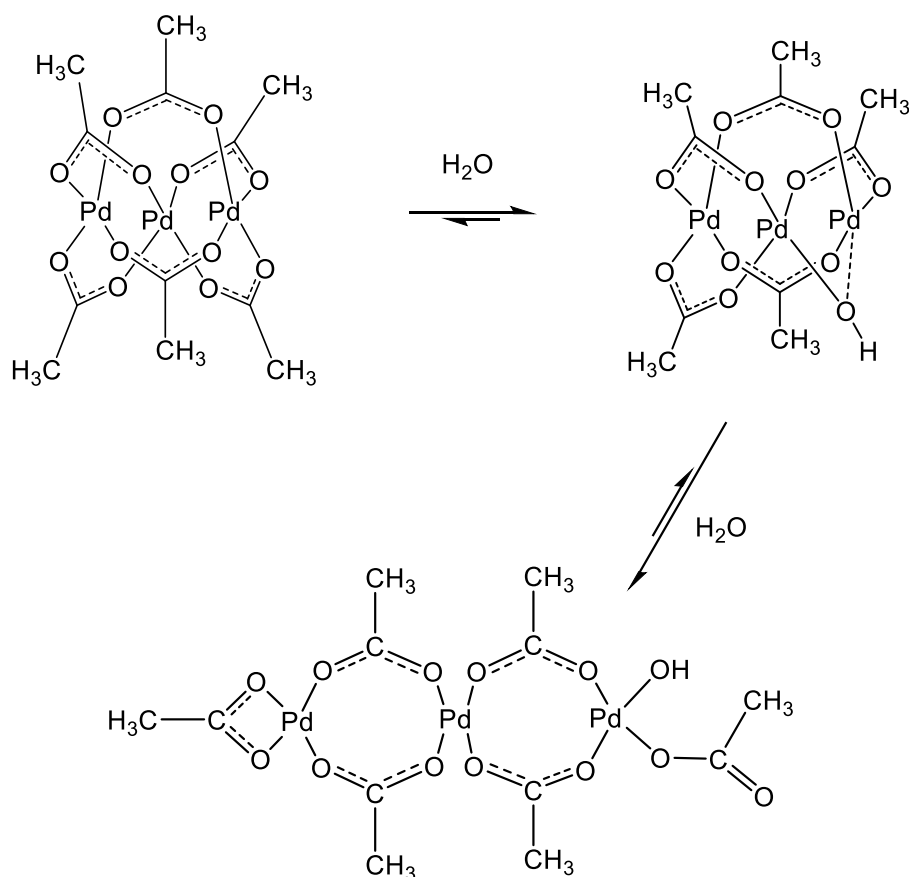


Fig. S10b. IR wavenumbers for (b) the C≡N stretching mode and (c) the O-D stretching mode as a function of increasing water mole fraction ($\chi_{\text{H}_2\text{O}}$) from $\chi_{\text{H}_2\text{O}} = 0.00$ to 1.0. The water contains 20 % D₂O and the MeCN:water mixtures contain 1 mM Pd-acetate + 0.1 M TBABF₄.



Scheme 1: Initial stage in perturbation of the Pd-acetate structure through the addition of water: Cage opening of the Pd acetate trimeric complex.⁹

ESI 6: Electrochemistry of Pd-acetate in different MeCN-water mixtures

Fig S11 shows (a) chronoamperometric data and (b) BDD electrode EDX surface analysis, post electrochemical reduction of Pd-acetate in water-MeCN solutions.

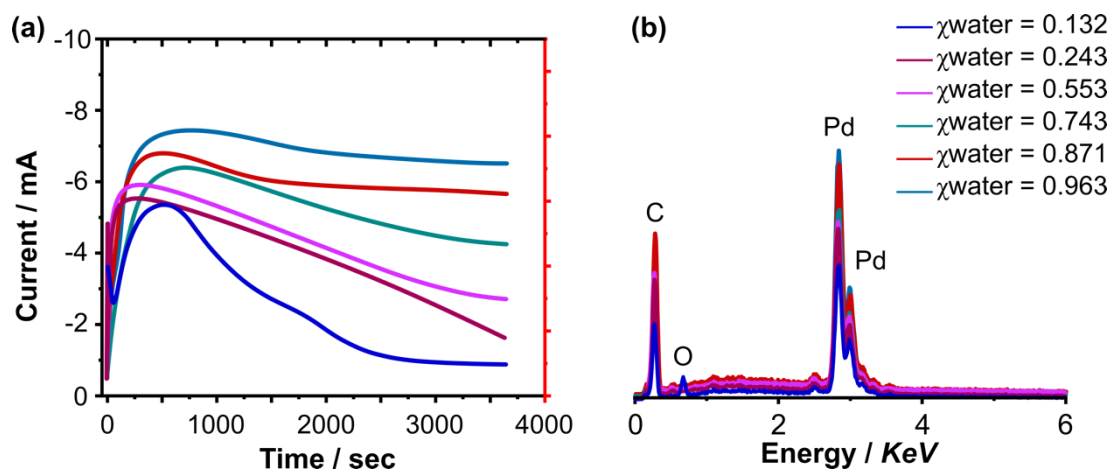


Fig. S11. Investigation of Pd electrodeposition from 1 mM Pd-acetate + 0.1 M TBABF₄ in various MeCN:water mixtures. (a) Chronoamperometric current-time profile. (b) EDX fingerprint of the Pd deposit on BDD.

ESI 7: Chemical synthesis of 4-acetylbiphenyl (Suzuki reaction)

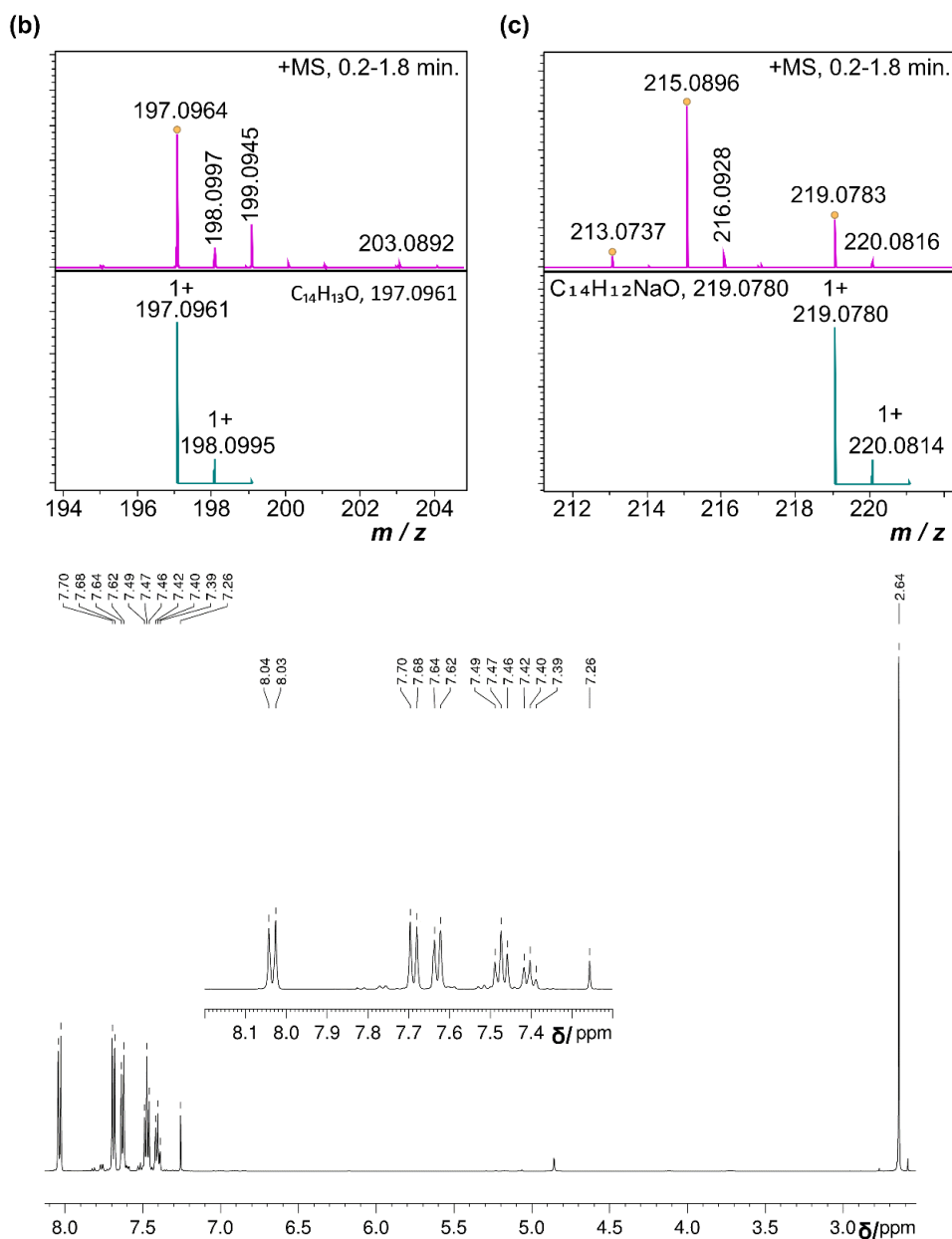
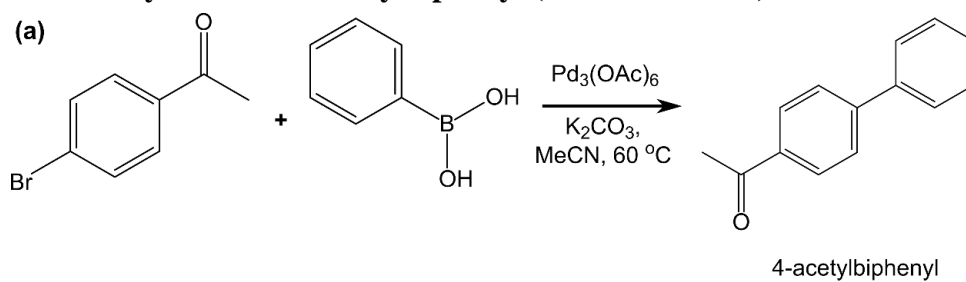


Fig. S12. (a) The Suzuki coupling reaction of 4'-bromoacetophenone with phenylboronic acid catalyzed by Pd-acetate in MeCN. (b and c) ESI-TOF-MS analysis of crude 4-acetylbiphenyl showing the molecule and its sodiated structure, respectively. (d) ^1H NMR spectrum of crude 4-acetylbiphenyl.

ESI 8: Electrochemical recovery of Pd from the synthesis solution

EDX (Fig. S13) and FE-SEM (Fig S14) analysis of the surface of the BDD RDE electrode post Pd recovery via electrodeposition, from the Pd-acetate containing synthesis solution, with 10% (v/v) water added.

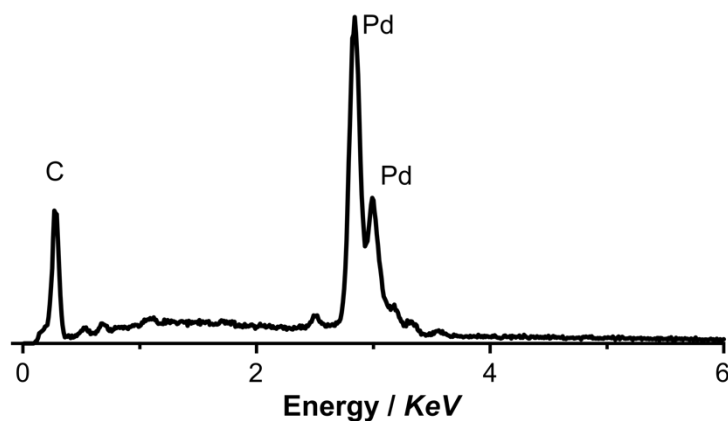


Fig. S13. EDX spectrum of Pd post the electrodeposition of Pd from the Suzuki coupling reaction solution containing 193 ppm Pd-acetate + 0.1 M TBABF₄ in MeCN:water mixed solvent, $\chi_{\text{MeCN}} = 0.757 + \chi_{\text{water}} = 0.243$ (90%:10% v/v) using a 25 mm diameter BDD RDE (1000 rpm).

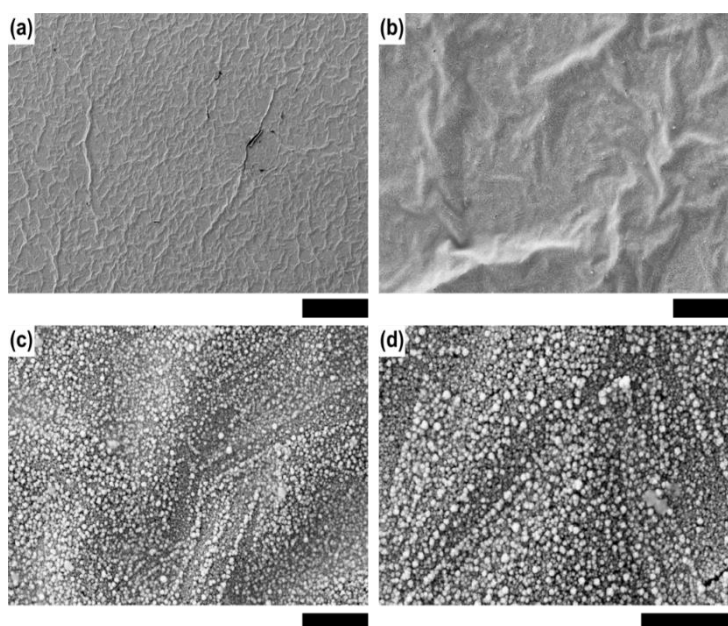


Fig. S14 a-d. In-Lens FE-SEM images at increasing resolution, of Pd metallic layer electrodeposited using double pulse potential steps at $\eta = -1$ V for $t_{\text{dep}} = 800$ s then at $\eta = -0.35$ V for $t_{\text{dep}} = 10,000$ s. Scale bar = (a) 200 μm, (b) 20 μm, (c) 2 μm, and (d) 2 μm.

ESI 9: Experimental, methodology and materials

Chemicals and solution preparation

The solutions were prepared with trace element grade chemicals, and all chemicals were used as received without further purification. 99.99% HPLC far UV-Vis grade MeCN and deionised water from a Purite Select HP system were used for solution preparation. Prior to each preparation, MeCN was dried over molecular sieves (3 Å, Merck chemicals) to ensure the absence of water. Pure 99.999% Ar and N₂ (BOC industries, UK) were used to de-aerate the solutions. For NMR studies, deuterated MeCN (MeCN-d₃) (99.999%, superseal, flushed and stored under Ar) and deuterium oxide (D₂O) were purchased from Acros organics.

Table S2: Composition of the solutions used in Pd solvation and electrodeposition study.

#	MeCN	H ₂ O	D ₂ O*	Pd-acetate	TBABF ₄	HCl	KCl	Mole fraction (χ_{water})
1	100%	0%	0%	1 × 10 ⁻³ M	0.1 M			0
2	95%	4%	1%	1 × 10 ⁻³ M	0.1 M			0.132
3	90%	8%	2%	1 × 10 ⁻³ M	0.1 M			0.243
4	80%	16%	4%	1 × 10 ⁻³ M	0.1 M			0.419
5	70%	24%	6%	1 × 10 ⁻³ M	0.1 M			0.553
6	60%	32%	8%	1 × 10 ⁻³ M	0.1 M			0.658
7	50%	40%	10%	1 × 10 ⁻³ M	0.1 M			0.743
8	40%	48%	12%	1 × 10 ⁻³ M	0.05M		0.05M	0.812
9	30%	56%	14%	1 × 10 ⁻³ M	0.04		0.06	0.871
10	20%	64%	16%	1 × 10 ⁻³ M	0.03		0.07	0.920
11	10%	72%	18%	1 × 10 ⁻³ M	0.02		0.08	0.963
12	5%	76%	19%	1 × 10 ⁻³ M	0.01		0.09	0.982
13	1%	79.2%	19.8%	1 × 10 ⁻³ M			0.1 M	0.997
14	0%	80%	20%	1 mM		0.1 M	0.05 M	1.000

Electrochemical studies

The reference electrode was constructed from a Ag wire immersed in a MeCN solution containing 0.1 M TBABF₄ and separated from a compartment containing the same solution by a porous Vycor tip (BASI). The latter compartment was in turn separated from the main solution by a second Vycor. Prior to each experiment, the BDD electrode (working electrode) was polished with alumina slurry (0.05 μm sized particle, micro polish, Buehler) on a DI water saturated polishing pad (Micro cloth, Nuehler, Germany) to obtain a mirror surface. This was followed by a polish on DI water saturated pad only to remove debris. The electrode was thoroughly rinsed with Milli-Q ultrapure water and dried under Ar and kept in a desiccator under vacuum.

The electrochemical setup is shown in Fig. S15. All voltammetry experiments were completed using organic media thoroughly degassed with Ar, under anaerobic conditions in a glovebox

(Plas Labs, Mich, US) filled with nitrogen ($O_2 < 7$ ppm, $H_2O < 2$ ppm) and at an ambient temperature of 22 ± 2 °C. CV and chronoamperometry (CA) were made using a 1 mm diameter BDD macrodisk electrode.

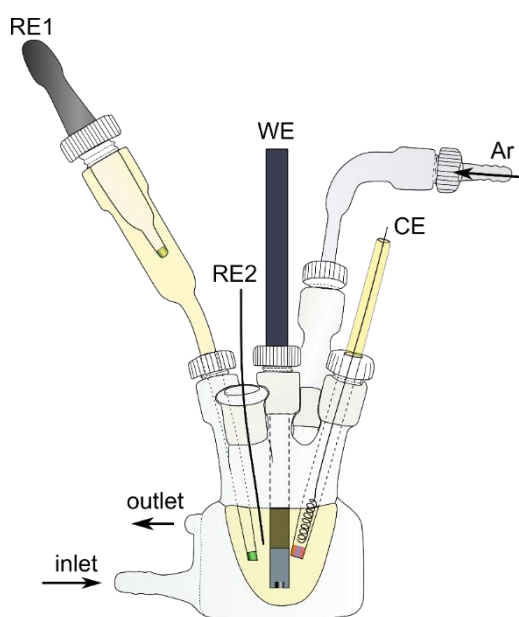


Fig. S15. Experimental set-up for the electrochemical studies of Pd systems

Microscopy Characterisation

Microscopic studies were carried out *ex-situ* after electrodeposition. After electrodeposition, the electrode was rinsed with de-oxygenated water, dried in the glove box and kept in a desiccator to avoid any contamination during transfer and prior imaging. For each deposition, at least three images were recorded in different areas of the surface for FE-SEM.

ESI 10: Notes and references

1. S. D. Kirik, R. F. Mulagaleev and A. I. Blokhin, *Acta Crystallographica Section C*, 2004, **60**, m449-m450.
2. V. I. Bakhmutov, J. F. Berry, F. A. Cotton, S. Ibragimov and C. A. Murillo, *Dalton transactions*, 2005, **11**, 1989-1992.
3. V. M. Nosova, Y. A. Ustynyuk, L. G. Bruk, O. N. Temkin, A. V. Kisin and P. A. Storozhenko, *Inorganic chemistry*, 2011, **50**, 9300-9310.
4. R. S. McDonald, *Analytical chemistry*, 1986, **58**, 1906-1925.
5. D. Jamroz, J. Stangret and J. Lindgren, *Journal of the American Chemical Society*, 1993, **115**, 6165-6168.
6. J. C. Hidalgo-Acosta, M. A. Mendez, M. D. Scanlon, H. Vrubel, V. Amstutz, W. Adamiak, M. Opallo and H. H. Girault, *Chemical Science*, 2015, **6**, 1761-1769.
7. J. R. Reimers and L. E. Hall, *Journal of the American Chemical Society*, 1999, **121**, 3730-3744.
8. T. Takamuku, M. Tabata, A. Yamaguchi, J. Nishimoto, M. Kumamoto, H. Wakita and T. Yamaguchi, *The Journal of Physical Chemistry B*, 1998, **102**, 8880-8888.
9. W. A. Carole and T. J. Colacot, *Chemistry European Journal*, 2016, **22**, 7686-7695